Diffusion-controlled and diffusionless crystal growth of tris-naphthylbenzene isomers in the supercooled liquid and glassy states

Author: Markus Seidl^{1,2}

Manuscript published in: Markus Seidl, Crystallization of glasses in the glass transition region,

Dissertation, Innsbruck, July 2015

This manuscript has not been published in a peer-reviewed journal due to personal differences with

Mark D. Ediger² as one of the anticipated co-authors. Shakeel S. Dalal² is another anticipated co-

author. Both have not reviewed the present manuscript.

¹Institut für Physikalische Chemie, Universität Innsbruck, Innrain 80–82, 6020 Innsbruck, Austria

²Department of Chemistry, University of Wisconsin–Madison, Madison, Wisconsin 53706,

United States

ABSTRACT

Before this work fourteen organic glass formers of low molecular mass have been known to exhibit an

extraordinary fast crystallization mode called GC growth which is activated near the glass transition

temperature $T_{\rm g}$. It reaches deep into the glassy state and displays a rich phenomenology, e.g., fast

growing fibers up to temperatures of $1.15 \cdot T_g$. It has been found that, contrary to diffusion-controlled

growth in the equilibrium liquid state, GC growth is not limited by diffusion. However, despite numer-

ous scenarios aiming at an explanation of this fast crystallization process its molecular mechanism still

remains unsolved. Here we study the influence of the molecular structure on the occurrence or absence

of the GC mode. In particular, we determine the crystallization kinetics of three tris-naphthylbenzene

(TNB) isomers in the supercooled liquid and glassy states. We find that α, α, α -TNB shows *steady-state*

fast bulk crystal growth at temperatures $\leq T_g$ as well as other features being associated with the exis-

tence of the GC mode. In contrast, α, β, β -TNB exhibits only *transient* fast bulk crystal growth below its

 $T_{\rm g}$. In the case of α, α, β -TNB we do not observe any indications for the existence of fast diffusionless

crystal growth at all. β, β, β -TNB has not been studied because it is a bad glass former. We propose that

a combination of our findings and the (yet unsolved) crystal structures of the TNB isomers provides

essential information on the way to resolve the mechanism underlying GC growth.

1

I. INTRODUCTION

In the glassy state materials' properties are tunable in a wide range due to the variable degree of structural disorder. This makes glasses useful for many applications, including electronics, biopreservation and pharmaceutics [1-5]. Accordingly, many physical properties differ to an even larger extent if a glassy material of a particular substance is compared to a crystalline, i. e., structurally ordered material of the same substance. For instance, the glassy state generally exhibits a larger solubility than the crystalline state, which is of great importance in the delivery of drugs to the organism [2]. Therefore, the stability of glasses against crystallization is not only of theoretical interest to gain a better understanding of crystal nucleation and growth, but also represents a crucial aspect of applied materials research.

In general, during crystallization of liquids and glasses the molecules have to re-orient to form the regular crystal lattice. In the liquid state, i.e. above the glass transition temperature T_g , crystallization is controlled by diffusion. In contrast, below T_g diffusion is too slow and, therefore, the crystallization of glasses must originate from other molecular processes. Very remarkably, in 1967, Greet and Turnbull reported for *ortho*-terphenyl that "at temperatures near the glass transition [...] at least parts of the crystallization front propagated at rates 3 to 4 orders of magnitude greater [...] than the limiting velocity calculated from the viscosity." [6] Their finding indicates that crystal growth even around T_g might not be controlled by diffusion. However, they did not provide an explanation for this fast crystal growth, and it still lacks understanding almost fifty years later.

Nowadays this mode of crystal growth is usually termed glass-to-crystal (GC) growth mode since it reaches deep into the glassy state. For *ortho*-terphenyl and indomethacin (which exhibits GC growth, too) it has indeed been confirmed to be "diffusionless" because its onset is not accompanied by an increase in the diffusion coefficient [7,8], see Figure 1 in Ref. [9]. So far, the GC mode has been found for fourteen single-component organic glass formers with molar masses ranging from 92 to 358 g/mol: *ortho*-terphenyl [6,10-12], salol [13,14], triphenylethylene [15,16], benzophenone [14], toluene [17], *iso*-propylbenzene [18], dimethyl phthalate [18], diphenyl phthalate [18], nifedipine [19], 5-methyl-2-[(2-nitrophenyl)amino]-3-thiophenecarbonitrile (ROY) [20-22], testosterone propionate [23], 1,2-diphenylcyclopentene [24], 1,2-diphenylcyclohexene [24] and indomethacin [9]. As described in this work, at least one *tris*-naphthylbenzene (TNB) isomer also exhibits GC growth, resulting in fifteen systems and an extended range of molar masses of up to 457 g/mol for which fast crystal growth in the glassy state has been found. We note that TNB exhibits the highest T_g (α , α , α -TNB: 73.0 °C) of all systems known to show GC growth so far.

Chemical characteristics being essential for this growth mode (e.g., the type of intra- and intermolecular interactions, respectively) have not been identified yet. Theories aiming at an explanation of GC growth are challenged by numerous observations characterizing this growth mode. The main feature is a sudden increase of bulk crystal growth rates by several orders of magnitude at the transition temperature T_t (which is typically slightly larger than T_g) upon cooling. This temperature is also called termination temperature since it is the highest temperature for which GC growth can be observed. Very recently it has been found that for temperatures $T \le T_t$ the ratio between the diffusivity D and the crystal growth rate u is ≤ 7 pm which appears to be a general condition for the GC mode to show up [9]. Hence, GC growth occurs when liquid diffusion is slow as compared to crystal growth, suggesting that it is terminated by fluidity at T_t. In addition to the abrupt onset or termination of GC growth, the following phenomena need to be rationalized by models for the GC mode: Fast crystal growth may appear at temperatures $T_t < T < 1.15 \cdot T_g$ in the form of fast growing fibers [9,12,18,20,23,25]. For ROY, the ends of such fibers are found to be preferred sites for the growth of new bulk GC crystals at temperatures below T_t [20]. After a certain time above T_t, GC growth may resume only at certain sites at the crystal/liquid interface [20]. Furthermore, the growth rate in the GC mode is found to slightly decrease with time both for ROY [22] and ortho-terphenyl [12]. The appearance or absence of GC growth, respectively, seems to depend on the degree of isotropy of the crystal polymorph that actually forms. Polymorphs with rather anisotropic packing of the molecules do not exhibit GC growth, while polymorphs with more isotropic packing, thus being structurally more "liquid-like" show GC growth [21]. Hence, structural similarities between the liquid (or glassy) state and the crystalline phase may be a pre-condition for the GC mode to occur.

Up to date five distinct scenarios have been developed aiming at an explanation of the GC growth mode. Oguni and co-workers proposed a mechanism named homogeneous-nucleation-based crystallization where enhanced nucleation near $T_{\rm g}$ is proposed to be at the bottom of GC growth [10,11]. Another approach frequently termed tension-induced mobility is given by Tanaka and co-workers. They consider the decoupling of translational diffusion from structural relaxation as well as enhanced molecular mobility due to greater free volume around crystal nuclei to enable the fast crystallization observed around $T_{\rm g}$ [26,27]. In contrast, Yu and co-workers consider the GC mode to be similar to crystal-crystal transformations, hence naming their scenario solid-state transformation enabled by local molecular motions [21]. Other scenarios propose percolative nanocrystallization [28] or mobility induced by shear stress [29] to cause GC growth. None of these approaches can account for all aspects of

the rich phenomenology of GC growth, and none of them establishes a solid basis to predict which materials show this crystal growth mode.

It is reasonable to expect that certain functional groups in the molecules influence the occurrence of GC growth, at least the magnitude of the growth rate. Indeed, based on the framework of homogeneous-nucleation-based crystallization and steric considerations, Oguni and co-workers were able to explain the maximum GC growth rate via bonding between phenyl rings [18]. However, the authors did not assume that the presence of phenyl rings is an inevitable prerequisite for the existence of GC growth. In fact, testosterone propionate does not have a phenyl ring but still exhibits GC growth [23]. Very recently, some of us reported on the crystal growth kinetics of 1,2-diphenylcyclopentene and 1,2-diphenylcyclohexene [24] which are structural analogs of *ortho*-terphenyl [30]. Around T_g , both of them crystallize in the GC mode just as *ortho*-terphenyl. However, yet another analog, 1,2-diphenylcyclobutene, exhibits only transient fast crystal growth near T_g which does not persist (cf. Sec. IV.A in this work).

Here we study the crystallization kinetics of three *tris*-naphthylbenzene (TNB) isomers in the liquid and in the glassy states to further elucidate the influence of the molecular structure on the appearance of GC growth. The Lewis structures of these isomers are shown in Fig. 1, highlighting the different positions on the naphthyl ring at which they are connected to the central benzene ring. The isomers considered in this work, i.e., $\alpha, \alpha, \alpha, \alpha$, α, α, β and α, β, β -TNB are good glass formers [31]. That is, they can easily be transformed from the liquid to the glass and vice versa [5]. In contrast, β, β, β -TNB is a bad glass former which easily crystallizes upon cooling of the melt [31]. Thus, we refrain from studies on this isomer. Nevertheless, all TNB isomers form glasses by vapor deposition where the appropriate substrate temperature of $0.85 \cdot T_g$ leads to glassy states of ultrahigh stability [32-34]. Very recently, one of us performed dielectric spectroscopy measurements on $\alpha, \alpha, \alpha, \alpha, \alpha, \alpha, \alpha, \beta$ - and α, β, β -TNB in their supercooled liquid state [33]. In the case of all three isomers, the obtained dielectric relaxation time $\tau_{\alpha}(T)$ shows non-Arrhenius behavior which can be fitted by the Vogel-Fulcher-Tammann (VFT) equation [35-37]

$$\log(\tau_{\alpha}/s) = A + \frac{B}{T - T_0} \tag{1}$$

Based on τ_{α} one typically defines the glass transition temperature to be given by $T_g=T(\tau_{\alpha}=100s)$. From this condition and Eq. (1) it then follows

$$T_{\rm g} = T_0 + \frac{B}{2 - A} \tag{2}$$

Tab. I provides the resulting T_g values (the fitting parameters A, B, and T_0 are reported in Tab. I of Ref. [33]) of the three isomers, which we consider throughout this work whenever we refer to the characteristic temperature of an isomer's glass transition.

The melt of α,α,β -TNB is a very well studied molecular liquid which has been characterized with respect to, e.g., volume, viscosity and glass forming ability [38-41] as well as heat capacity [41,42]. Furthermore, its crystallization kinetics have been determined and analyzed within a broad temperature region ($T_{\rm g} < T < T_{\rm m}$) [41,43-45]. Therefore, we are able to compare our results on the crystallization kinetics of α,α,β -TNB with literature (Fig. 2) to judge the quality of our material and to evaluate the performance of our experimental setup and protocol.

II. EXPERIMENT

A. Sample preparation and characterization

In the studies reported here we used TNB samples with a thickness of about 10–20 µm, being enclosed between two cover glasses made from boro silicate glass (thickness: 0.13–0.16 mm, diameter: 15 mm; Ted Pella, Inc.). The raw material was provided by Laura Kopff and Robert McMahon (Department of Chemistry, University of Wisconsin–Madison). As a purification step we vaporized the as-obtained material and deposited it directly on a cover glass kept at room temperature; in this procedure a *glass with ultrahigh stability* is gained [32]. The sample was then heated on our temperature control stage (see below) to form a liquid. The liquid material was then covered with another cover glass and subsequently cooled to room temperature where an *ordinary glass* is gained.

For the crystallization studies the glassy sample was seeded from the side using crystals taken from the raw material and then kept at a certain temperature above $T_{\rm g}$. Once that a large enough fraction of crystalline material had formed we could determine the melting point in a step-wise heating process (typical temperature increment: 1 °C; typical waiting time at each temperature: 5 min) by visually observing the crystals in our optical microscope (see below). The respective melting temperatures $T_{\rm m}$ can

be found in Tab. I where we also list literature values for comparison. Relative to the latter values our own results deviate by $\pm 1.4\%$ at most. Throughout this work we consider the $T_{\rm m}$ values obtained by visual inspection whenever we refer to the melting temperature.

In the case of α , α , α - and α , α , β -TNB, respectively, we prepared only one sample. However, in the case of α , β , β -TNB we prepared two samples to check for the general reproducibility of the preparation procedure. The two samples show the same melting temperature and their growth rates match each other very well (hence, data from both samples are reported in Sec. III.B), thus confirming the preparation to be reproducible.

B. Optical microscope and temperature control stage

Our investigation of crystal growth kinetics as a function of temperature is based on photomicrographs capturing the crystal growth front with time. For this purpose we use an optical light microscope (Olympus, model BX51TRF) equipped with different lenses of 4-, 10- and 20-fold magnification, respectively, polarization filters and a digital camera. Using the lens with 20-fold magnification, the distance covered by the crystal growth front advancing into the liquid (or glassy) part of the sample has to be at least $\approx 10~\mu m$ to result in a reliable growth rate. This distance is used to calculate the upper limit of the growth rate for cases where no crystal growth is observed.

The sample rests on the thermostated metal block of a temperature-control stage (Linkam, model THMSE 600) which is mounted onto the table of the microscope. The temperature of the stage is measured with an internal sensor and is accurate to at least ± 0.1 °C.

In principle, this stage allows for measurements in the transmitted light mode of the microscope because the metal block has an orifice with a diameter of 2 mm in the middle where the light can pass through. However, we noticed that at least for temperatures ≥100 °C a thermal gradient from the massive block across the orifice exists which we estimate to be around 4 °C at 140 °C. Of course, this gradient increases with an increase in the temperature difference between the thermostated metal block and its environment. Therefore we followed crystal growth in a part of the sample which was not kept over the orifice of the metal block but directly over the massive metal instead. For this reason we run the microscope in the reflected light mode. The only disadvantage of this protocol (as compared to the transmitted light mode) was that the photomicrographs show the metal block in the background (Fig. 3)

which makes it more difficult to see the crystal growth front if the polarization filters are not used, especially in the case of a large depth of focus.

C. Determination of crystal growth rates

The samples were kept isothermally at temperatures from close to the melting temperature $T_{\rm m}$ down to the glass transition region to follow crystal growth. In particular, α , α , α -TNB was studied from 60 °C $(0.96 \cdot T_{\rm g})$ to 175 °C $(1.29 \cdot T_{\rm g})$ or $0.98 \cdot T_{\rm m}$, α , α , β -TNB from 55 °C $(0.95 \cdot T_{\rm g})$ to 190 °C $(1.34 \cdot T_{\rm g})$ or $0.99 \cdot T_{\rm m}$ and α , β , β -TNB from 55 °C $(0.97 \cdot T_{\rm g})$ to 145 °C $(1.24 \cdot T_{\rm g})$ or $0.98 \cdot T_{\rm m}$.

The crystal growth rate at a certain temperature u(T) is defined as $\Delta l/\Delta t$ where Δl is the distance covered by the crystal growth front advancing into the liquid (or glassy) part of the sample in time Δt . The rates reported in this work are mean values based on individual rates obtained for 2-4 growth sites. Depending on the growth morphology a growth site can be a single crystal or a spot of a polycrystalline growth front (cf. Fig. 3 and Fig. 4). In general, the preferred growth morphology changes with temperatures as indicated in Fig. 5. However, a crystal growth front composed of crystals with a particular morphology continues to grow in its present form at least for some time if the sample is brought to a temperature at which a different morphology is preferred. This is due to the fact that, depending on the actual temperature, the growth morphology needs some time to change to the preferred morphology. As a consequence we were able to determine growth rates at a certain temperature for crystals growing in another than the preferred morphology, too. We took advantage of this both in the case of α , α , α - and α, α, β -TNB, while we followed the growth of single crystals only in the case of α, β, β -TNB because polycrystalline growth fronts above $T_{\rm g}$ were less developed here. However, we have followed both growth rates exhibited by single crystals and by spots of a polycrystalline growth front, respectively, down to a temperature of 145 °C (115 °C) in the case of α , α , α -TNB (α , α , β -TNB). For this temperature region we did not recognize a significant difference in the growth rates exhibited by these two crystal growth morphologies. At lower temperatures we followed the growth of single crystals only. As discussed below (Sec. III), growth of fast crystalline spikes and fibers is observed below ≈120 °C for α , α , α -TNB. We could not evaluate their respective growth rate because of their twisted or curled shape, but their growth was accompanied by a bulk-like growth at the interface to crystals grown at higher temperatures. Hence, we calculated the growth rate for this (polycrystalline) region in addition to the single crystal's growth rate.

Between measurements at different temperatures we cooled the sample to room temperature which led to the formation of cracks in the crystalline material, presumably because of thermal strain. Such cracks appear as black lines in the crystalline phase, see Fig. 3. They are oriented tangentially to the growth direction or, in other words, parallel to the growth front. Characteristic points along cracks or along borders of single crystals (Fig. 3, radially oriented black lines in the crystalline phase) as well as intersection points of cracks and crystal borders acted as time-independent reference points from which Δl was measured as a function of time.

To obtain significant crystal growth at the lowest temperatures considered in this work, i. e., around $T_{\rm g}$ (55, 60 and 73°C, respectively), the samples were kept at the respective temperature from several days to several months. For this purpose we stored the samples in thermostated ovens. The temperature was not recorded with time, but occasional inspection of the actual temperature indicated a temperature accuracy of ± 0.1 °C. Potential crystal growth was evaluated by taking the respective sample out of the oven and subsequently recording photomicrographs at room temperature.

In Fig. 2 we compare our results on the crystallization kinetics of α , α , β -TNB to those obtained by Magill and Plazek [41,44]. It can readily be seen that the crystal growth rates u(T) obtained in the two studies are in excellent agreement. This indicates that the purity of the material under scrutiny is high and that sample temperature is reliable.

III. RESULTS

A. Morphology of crystal growth

The sequence of photomicrographs in Fig. 3(b) shows how the growth morphology of α , α , β -TNB changes with temperature. For small supercooling $\Delta T = T_{\rm m} - T$ of ≤ 25 °C (i. e., for temperatures just below $T_{\rm m}$) this isomer favorably grows in the form of faceted single crystals. The temperature region where this morphology is realized preferentially is marked by fsc in Fig. 5(b). For larger supercooling ΔT compact growth is observed, where the morphology changes from single crystals (csc in Fig. 5(b)) to dense fibers (df in Fig. 5(b)) with increasing ΔT . We do not observe any crystal growth around $T_{\rm g}$ in the case of α , α , β -TNB: The absence of measureable crystal growth in the sample kept at 60 °C \approx 0.97· $T_{\rm g}$ (55 °C \approx 0.95· $T_{\rm g}$) for 150 days (11 days) implies $\log[u/({\rm m~s^{-1}})] < -12.1$ (-11.0). The growth phenomenology observed by us coincides with the findings by Magill and Plazek [44] for the same isomer [41].

 α, β, β -TNB again shows a temperature-dependent crystal growth morphology where faceted single crystals represent the preferred morphology just below T_m, while compact growth of single crystals or dense fibers occurs in the case of larger supercooling ($\Delta T \ge 21$ °C), see Fig. 5(c). If crystallization develops from a small nucleus, pairs of crystals opposed to each other form, where the number of crystals may be only two or higher. This leads to the appearance of star-like arrangements, see the top photomicrograph in Fig. 3(c). Between $1.08 \cdot T_g$ and $1.13 \cdot T_g$ we observe spikes (see the third photomicrograph from the top in Fig. 3(c)) which are reminiscent of the growth morphology of α , α , α -TNB at, e.g., 1.12 T_g (see the second photomicrograph from the top in Fig. 3(a)). However, the formation of spikes is much less pronounced here. Again similar to the case of α, α, α -TNB, α, β, β -TNB exhibits fine-structured bulk crystal growth in the glass transition region (see the photomicrograph at the bottom of Fig. 3(c)). It is also fast as compared to the results gained for higher temperatures, see Fig. 5(c), but contrary to the case of α , α , α -TNB it dramatically slows down with time in the case of α , β , β -TNB: First the sample had been kept at 60 °C for 46 days after which it was brought to room temperature for microscopic inspection. From this crystal growth measurement one obtains $\log[u/(\text{m s}^{-1})]=-9.7$, see the respective data point shown in Fig. 5(c). Subsequently the sample was kept again at 60 °C for another 35 days, followed by microscopic inspection at room temperature. For this time interval one obtains $\log[u/(\text{m s}^{-1})]=-10.7$, see the respective data point shown in Fig. 5(c). Finally, the sample was kept at 60 °C for another 21 days, after which microscopic inspection did not reveal further crystal growth which implies $\log[u/(\text{m s}^{-1})] < -11.3$. After subsequent storage of the sample at 55 °C for 11 days again no crystal growth was observable, implying $\log[u/(\text{m s}^{-1})] < -11.0$.

We close the phenomenological description of the morphology of crystal growth by taking a closer look at α , β , β -TNB crystals grown at 60 °C. Fig. 4(b) shows a part of the sample where single crystals formed at high temperature made the initial crystal-glass interface available from where the growth of fine-structured crystalline material at 60 °C started. In the middle and right part of the photomicrograph domains with a length of up to >200 μ m starting from the single crystals are evident. However, this morphology then changed, resulting in smaller domains, and it does not appear everywhere, see the left part of the photograph.

B. Crystal growth rates

Fig. 5 shows the logarithm of the crystal growth rate u as a function of temperature. As already stated in the previous section we observe fast crystal growth around T_g and below both in the case of α, α, α -TNB and α, β, β -TNB (full symbols at $T \le T_g$ in Fig. 5(a) and (c)). In the former case we refer to it as GC growth because it occurs as steady-state growth, while in the latter case we refer to it as GC-like or transient fast growth because it slows down dramatically. The decrease in u with time is evident from the two largely differing data points at 60 °C, see Fig. 5(c), where the upper one refers to an earlier stage at this temperature than the lower one as already discussed above.

In addition to GC growth at $T \le T_g$ we find that certain locations of the α, α, α -TNB sample exhibit somewhat enhanced crystal growth kinetics as compared to the normal growth, see the asterisks in Fig. 5(a) and the corresponding photomicrographs in Fig. 6. Crystal growth at these locations appears to result in a dense crystalline phase. However, we want to emphasize that this kind of crystal growth is observed at growth fronts from which fast growing spikes or fibers emanate. In fact, it only occurs in the temperature range where these features are observed, i. e., at $T_g < T < 1.15 \cdot T_g$. Due to the apparent relationship between the phenomenon of loose fibers and enhanced (seemingly) space-filling crystal growth, respectively, we have to be aware that the latter might not be completely space-filling. Data for the normal growth mode in this temperature range are gained by the growth of single crystals.

For α, α, β -TNB we do not observe any indication for the existence of fast crystal growth near T_g at all. However, we cannot exclude its existence, but from our experiments it follows that u would have to be much smaller than in the case of the other two isomers, e.g., $\log[u/(\text{m s}^{-1})] < -12.1$ at 60 °C. (Here we

presume that if fast crystal growth exists it would immediately start at the respective temperature, i.e., without any time lag.)

Crystals growing in the normal mode are controlled by molecular diffusion or, in other words, diffusion is the molecular process limiting crystal growth at high temperatures. However, the as-measured growth rate u(T) does not directly reflect diffusion, i. e., the coefficient D(T), because not every contact of a molecule from the liquid with a proper growth site of the crystalline phase leads to its incorporation into the crystalline phase. Thermodynamics accounts for this effect: The driving force of crystal growth, defined by the difference of the Gibbs energies of the liquid and the crystalline phase (ΔG), determines the probability of molecules irreversibly attaching from the liquid to a crystalline phase. Hence, in order to gain information on molecular diffusion from the crystal growth data we have to consider the kinetic part of the crystal growth rate $u_{\rm kin}$. It is calculated via

$$u_{\rm kin} = \frac{u}{1 - e^{-\Delta G/(RT)}} \approx \frac{u}{1 - e^{-\Delta S_{\rm m}\Delta T/(RT)}} = \frac{u}{1 - e^{-\Delta H_{\rm m}\Delta T/(T_{\rm m}RT)}}$$
 (3)

where $\Delta G \approx \Delta S_{\rm m} \cdot \Delta T$ and $\Delta S_{\rm m} = \Delta H_{\rm m}/T_{\rm m}$ are used. Here $\Delta H_{\rm m}$ and $\Delta S_{\rm m}$ are the melting enthalpy and entropy, respectively, $T_{\rm m}$ is the melting temperature and $\Delta T = T_{\rm m} - T$ is the supercooling. The values of these quantities are provided in Tab. I; please note that we have used $\Delta H_{\rm m}$ and $T_{\rm m}$ from the references provided in footnote (d) of the table.

The kinetic part of the crystal growth rate is plotted in Fig. 5 in the form of colored symbols. The correction for the thermodynamic driving force is small at low temperatures where ΔT and ΔG are large, and it increases with increasing temperature. Since the accuracy of the correction might decrease with increasing temperature, we only consider data of $u_{\rm kin}$ up to a certain maximum temperature for which we apply the following two criteria: We do not plot data where (i) the uncorrected growth rate u is within a factor of 3 of the maximum growth rate or (ii) where the corrected growth rate u is larger than two times the uncorrected u.

IV. DISCUSSION AND CONCLUSIONS

A. Fast crystal growth

For α, α, α -TNB we find fast dense crystal growth with a fine structure at $T \le T_g$, i.e., the GC growth mode exists in the case of this isomer. Furthermore, it also shows other typical features being associated with the GC growth mode, namely fast growing loose domains up to $\approx 1.15 \cdot T_g$, see the respective indications (If and s) in Fig. 5(a). Close to this temperature they have the form of spikes, see the photomicrograph taken at $1.12 \cdot T_g$ in Fig. 3(a). These spikes are bent and resemble the fast growing loose domains found for testosterone propionate at $1.08 \cdot T_g$, see Fig. 8 in Ref. [23]. In contrast, fast growing spikes occurring in ortho-terphenyl at $1.11 \cdot T_g$ are straight as evident from Fig. 1(a) in Ref. [12]. Growth of spikes occurs also in the case of dimethyl phthalate at $1.07 \cdot T_g$, see Fig. 3(b) in Ref. [18], and in the case of nifedipine at $1.09 \cdot T_g$ or $1.06 \cdot T_g$, see Figs. 5(b) and 5(c) in Ref. [19]. All of these systems show space-filling fast crystal growth, i.e., GC growth around and below $T_{\rm g}$. For α, α, α -TNB we furthermore find that the fast growing loose domains change from spike-shaped to fiber-like at lower temperatures as evident from the photomicrograph taken at $1.08 \cdot T_g$ in Fig. 3(a). Again, a very similar behavior is found for testosterone propionate at 1.02·T_g (see Fig. 4(a) in Ref. [23]), ortho-terphenyl at $1.05 \cdot T_g$ (see Fig. 1(b) in Ref. [12]) and nifedipine at $1.03 \cdot T_g$ (see Fig. 5(d) in Ref. [19]). In addition, fast growth of fine loose fibers is reported for diphenyl phthalate around T_g , see Fig. 5(b) in Ref. [18], and ROY at 1.07-T_g or 1.04-T_g, see Figs. 3(b) and 4(a) in Ref. [20]. [Please note that Hatase et al. assigned the fast growing fibers (they name them "hair-shape" crystals) in diphenyl phthalate to normal or ordinary crystal growth [18], while Sun et al. found that such fibers in ROY connect GC and ordinary growth, respectively [20]. However, comparison of the growth rates shown in Fig. 6 in Ref. [18] and those shown in Figure 2 in Ref. [20] reveal the similarity between both systems.] Hence, α, α, α -TNB represents a typical system for which GC growth exists, making it the fifteenth known today to show GC growth. No molecule of higher molar mass and higher T_g is known to exhibit this phenomenon.

In the case of α , α , α -TNB, a close look at the growth front from which fast growing spikes or fibers emanate (Fig. 6) suggests that there might be dense crystal growth (asterisks in Fig. 5(a)) which is by a factor of 2–3 faster than growth in the normal mode (open circles in Fig. 5(a)). However, it could also be that this part of the crystalline phase consists of spikes or fibers which are too small to be resolved

with our setup. That is, at present it remains open whether or not the crystalline phase is indeed a space-filling precursor of GC growth.

Furthermore, for α , α , α -TNB we find that the GC growth mode (at 60 °C) resumes only at some locations at the crystal-glass interface when its activity is first stopped by *cooling* to room temperature and then aimed to be reactivated by heating to 73 °C, see Fig. 4(a). For the system of ROY it was found that *heating* actively growing GC crystals into the regime where the GC growth is not observed anymore can irreversibly deactivate the GC mode. This means that GC growth resumes only at parts of the crystal-liquid interface after cooling the sample back into the GC growth regime. However, we are not aware that a deactivation of GC growth by exposure to low temperatures as found for α , α , α -TNB has been reported before. We are not able to provide an explanation for this finding.

While we did not find any indications for the appearance of GC growth in α,α,β -TNB (Figs. 3(b) and Fig. 5(b)), fast crystal growth is also observed in the case of α,β,β -TNB. However, in contrast to α,α,α -TNB which shows a number of signatures characteristic for the existence of the GC mode, α,β,β -TNB is different from "classical" GC systems. First we do not find loose fibers above T_g in the case of this isomer. As shown in Fig. 3(c) (third photomicrograph from above) only small spikes appear which stop their longitudinal growth at some point and thicken instead, acting as a kind of protuberances of the normal growth mode. Nevertheless, we find GC-like fine-structured bulk crystal growth near T_g also for α,β,β -TNB, see the photomicrograph at the bottom of Fig. 3(c) and Fig. 4(b). However, we refrain from calling it GC growth because it dramatically slows down with time as illustrated by the two data points at 60 °C in Fig. 5(c) which refer to the crystal growth in different time intervals.

Very recently some of us have reported a very similar GC-like crystallization behavior for 1,2-diphenylcyclobutene (DPCB); please refer to the Supporting Information of Ref. [24]. DPCB exhibits transient fast crystal growth near and below T_g , forming a crystalline phase with grain-like morphology. It exhibits a constant growth rate at the beginning of glass crystallization (at 215 K: $\log[u/(\text{m s}^{-1})]\approx-7.2$), which then slows down. It was considered that crystal growth in fact stops completely, but Fig. S8 in the Supporting Information of Ref. [24] (showing the distance of crystal growth vs. time) suggests a finite growth rate after the slow-down at least at a temperature of 215 K for which $\log[u/(\text{m s}^{-1})]\approx-9.7$ is found. Unfortunately, in this figure there are not enough data to recognize how the two linear regimes are connected to each other. That is, there might be a rather sharp kink or a more or less rounded progression of the curve. Our results for α,β,β -TNB at 60 °C coincide with those for DPCB, even though

we have to be aware that due to the generally slow kinetics of this TNB isomer we evaluated u only for two time intervals. For the first time interval (from day 0 to day 46) we find $\log[u/(\text{m s}^{-1})]$ =-9.7 (upper data point in Fig. 5(c)) which could represent the rate of GC-like growth. For the third time interval (from day 81 to day 102) we find that $\log[u/(\text{m s}^{-1})] < -11.3$ because no growth could be observed within this interval. Hence, crystal growth could still take place but, however, with a rate at least \approx 2 orders of magnitude smaller compared to the GC-like growth. For DPCB the relation of the growth rates of the fast transient and slow temporal regime at 215 K reveals 2–3 orders of magnitude, being in agreement with our speculation. For the intermediate, i.e, second time interval of our experiment on α,β,β -TNB at 60 °C (from day 46 to day 81) we find $\log[u/(\text{m s}^{-1})]$ =-10.7 which suggests that the change from fast to slow kinetics lies in this time interval. Of course, further experiments would be necessary to clarify whether α,β,β -TNB indeed shows a similar change in the crystallization kinetics as DPCB rather than, e.g., a continuous slow down of the crystallization rate.

B. Diffusion-controlled and diffusionless crystal growth

The dielectric relaxation time τ_{α} generally represents the time scale of structural relaxation [46]. Therefore, comparison of our data on crystal growth with τ_{α} reveals whether or not crystallization is correlated with relaxation or diffusion. For this purpose we consider the time within which the crystal grows by one molecular layer, τ_u , as a measure for the time scale of crystal growth. It is given by $\tau_u = a/u$, where a=9.7 Å is the molecular diameter of TNB [22] and u is the crystal growth rate as measured.

Fig. 7 shows both τ_{α} and τ_{u} of the three TNB isomers in the form of an Arrhenius plot. Comparison of the time scale of liquid relaxation and crystal growth, respectively, clearly shows that two distinct modes of crystal growth are found. At the high-temperature side (small values for T_g/T), the time required for the crystal to grow one molecular layer (τ_u , empty symbols and asterisks) is larger than the time required for the liquid to relax (τ_{α}). Therefore, at high temperatures crystal growth is controlled by diffusion which correlates with τ_{α} (for a quantitative description of this correlation see below). Contrary to this normal crystal growth, at the low-temperature side (large values for T_g/T) the time required for the crystal to grow one molecular layer (τ_u , full symbols) is smaller than the time required for the liquid to relax (τ_{α}). That is, below the glass transition temperature T_g (where $T_g/T=1$) crystal growth is not governed by diffusion. This diffusionless mode of crystal growth is found for α, α, α - and α, β, β -

TNB, but not for α, α, β -TNB. Hence, the molecular geometry indeed influences the appearance or absence of fast crystallization in glasses.

It is of further interest to directly compare the time scale of diffusion-controlled crystal growth to the time scale of relaxation in the equilibrium liquid, see the upper part of each panel in Fig. 8. There we plot both quantities on a logarithmic scale, where τ_u is calculated using the growth rate as measured (u, gray symbols) or the kinetic part of the growth rate (u_{kin} , color symbols). We consider the latter to illustrate the relation between diffusion and relaxation, while the former only serves to illustrate the effect of the correction to the thermodynamic driving force. In the case of all isomers all data points lie above the dashed line defined by $\log(\tau_u/s) = \log(\tau_0/s)$, i.e., τ_u is larger than τ_α . The data are represented very well by a linear fit with slope ξ (solid line), i.e., the two time scales are connected via the power-law relation $\tau_u \propto \tau_\alpha \xi$. The parameter ξ characterizes the degree of decoupling of crystal growth kinetics from liquid relaxation.

The values obtained for ξ are provided in Fig. 8 as well as in Tab. I. For α,α,β -TNB we find ξ =0.743±0.005. If the growth rates u_{kin} [41,44] (instead of τ_u) and the viscosity η [39] (instead of τ_α) are considered an analogous power-law relation $u_{kin} \propto \eta^{-\xi}$ with the same value ξ =0.74 is gained [45,47]. This reflects the well-known finding that τ_α and η show very similar temperature dependencies [46,48]. Furthermore, the self-diffusion coefficient D_T correlates with η in a very similar manner as u_{kin} , namely by $D_T \propto \eta^{-\xi}$ with ξ =0.77 [49]. From this it follows that the crystallization of supercooled liquid α,α,β -TNB is indeed controlled by translational diffusion, i.e., $u_{kin} \propto D_T$. In the case of α,α,α -TNB (α,β,β -TNB) we find $\tau_u \propto \tau_\alpha^{\xi}$ with ξ =0.81±0.03 (ξ =0.64±0.02). We want to emphasize that based on u_{kin} and η the exponent ξ □ is found to correlate with the liquid fragility m (the steepness index), where a single linear function accounts for the dependence in both inorganic and organic species, see Fig. 3 in Ref. [47]. The three TNB isomers follow this correlation as can be seen from the ξ and m values listed in Tab. I. One well-known consequence of the decoupling of crystal growth kinetics (u_{kin} , D_T) from the dielectric relaxation time τ_α (or from the viscosity η) is the so-called breakdown of the Stokes-Einstein equation [47,49-51]. It is frequently attributed to be due to increasing heterogeneous dynamics upon approaching the glass transition temperature T_g [52,53].

C. Conclusions

Based on our study of three TNB isomers we find that the molecular structure indeed influences the appearance or absence of fast crystallization in glasses: α, α, α -TNB shows steady-state fast bulk crystal growth at temperatures $\leq T_g$, i. e., the GC growth mode exists for this isomer. Furthermore, it also exhibits fast growth of loose spikes and fibers below $\approx 1.14 \cdot T_g$, a typical precursor of GC growth. α, β, β -TNB seemingly exhibits only *transient* GC-like crystal growth below its T_g , while no indication for GC or GC-like growth is found for α, α, β -TNB.

These findings represent valuable information to improve existing scenarios (or to establish new ones) aiming at an explanation of the GC growth mode [21]. It is now essential to solve the isomer's crystal structures (which are unknown up to date) because both the actual connectivity within the molecules as well as their structural details in the crystal lattice are required to further move towards the discovery of the mechanisms underlying the puzzling fast crystallization around $T_{\rm g}$.

ACKNOWLEDGMENTS

The authors thank Laura Kopff and Robert McMahon for providing us with the TNB isomers, C. Travis Powell for helpful advice concerning sample preparation and crystal growth measurement, Alfonso Sepúlveda for help with physical vapor deposition, Lian Yu for helpful discussions and Thomas Loerting for a critical reading of the manuscript. Support by the Austrian Federal Ministry of Science, Research and Economy (Marietta Blau fellowship of the OeAD-GmbH to M.S.) is gratefully acknowledged.

REFERENCES

- [1] J. H. Crowe, J. F. Carpenter, and L. M. Crowe, Annu. Rev. Physiol. **60**, 73 (1998).
- [2] L. Yu, Adv. Drug Delivery Res. 48, 27 (2001).
- [3] Y. Shirota, J. Mater. Chem. 15, 75 (2005).
- [4] A. De Silva, N. M. Felix, and C. K. Ober, Adv. Mater. **20**, 3355 (2008).
- [5] M. D. Ediger and P. Harrowell, J. Chem. Phys. 137, 080901 (2012).
- [6] R. J. Greet and D. Turnbull, J. Chem. Phys. 46, 1243 (1967).

- [7] M. K. Mapes, S. F. Swallen, and M. D. Ediger, J. Phys. Chem. B 110, 507 (2006).
- [8] S. F. Swallen and M. D. Ediger, Soft Matter 7, 10339 (2011).
- [9] D. Musumeci, C. T. Powell, M. D. Ediger, and L. Yu, J. Phys. Chem. Lett. 5, 1705 (2014).
- [10] T. Hikima, Y. Adachi, M. Hanaya, and M. Oguni, Phys. Rev. B 52, 3900 (1995).
- [11] T. Hikima, M. Hanaya, and M. Oguni, J. Non-Cryst. Solids 235-237, 539 (1998).
- [12] H. Xi, Y. Sun, and L. Yu, J. Chem. Phys. **130**, 094508 (2009).
- [13] T. Hikima, M. Hanaya, and M. Oguni, Solid State Commun. 93, 713 (1995).
- [14] M. Hanaya, T. Hikima, M. Hatase, and M. Oguni, J. Chem. Thermodyn. 34, 1173 (2002).
- [15] T. Hikima, N. Okamoto, M. Hanaya, and M. Oguni, J. Chem. Thermodyn. 30, 509 (1998).
- [16] T. Hikima, M. Hanaya, and M. Oguni, J. Mol. Struct. **479**, 245 (1999).
- [17] M. Hatase, M. Hanaya, T. Hikima, and M. Oguni, J. Non-Cryst. Solids 307-310, 257 (2002).
- [18] M. Hatase, M. Hanaya, and M. Oguni, J. Non-Cryst. Solids 333, 129 (2004).
- [19] H. Ishida, T. Wu, and L. Yu, J. Pharm. Sci. 96, 1131 (2007).
- [20] Y. Sun, H. Xi, M. D. Ediger, and L. Yu, J. Phys. Chem. B 112, 661 (2008).
- [21] Y. Sun, H. Xi, S. Chen, M. D. Ediger, and L. Yu, J. Phys. Chem. B **112**, 5594 (2008).
- [22] Y. Sun, H. Xi, M. D. Ediger, R. Richert, and L. Yu, J. Chem. Phys. 131, 074506 (2009).
- [23] A. Shtukenberg, J. Freundenthal, E. Gunn, L. Yu, and B. Kahr, Cryst. Growth Des. 11, 4458 (2011).
- [24] C. T. Powell, K. Paeng, Z. Chen, R. Richert, L. Yu, and M. D. Ediger, J. Phys. Chem. B 118, 8203 (2014).
- [25] Please note that Hatase et al. assigned the fast growing fibers (they name them "hair-shape" crystals) in diphenyl phthalate to normal or ordinary crystal growth [18], while Sun et al. found that such fibers in ROY connect GC and ordinary growth, respectively [20]. However, comparison of the growth rates shown in Fig. 6 in Ref. [18] and those shown in Figure 2 in Ref. [20] reveal the similarity between both systems.
- [26] H. Tanaka, Phys. Rev. E **68**, 011505 (2003).
- [27] T. Konishi and H. Tanaka, Phys. Rev. B **76**, 220201 (2007).
- [28] J. D. Stevenson and P. G. Wolynes, J. Phys. Chem. A 115, 3713 (2011).
- [29] C. Caroli and A. Lemaitre, J. Chem. Phys. 137, 114506 (2012).
- [30] W. Ping, D. Paraska, R. Baker, P. Harrowell, and C. A. Angell, J. Phys. Chem. B 115, 4696 (2011).
- [31] C. M. Whitaker and R. J. McMahon, J. Phys. Chem. **100**, 1081 (1996).

- [32] K. Dawson, L. Zhu, L. A. Kopff, R. J. McMahon, L. Yu, and M. D. Ediger, J. Phys. Chem. Lett. 2, 2683 (2011).
- [33] K. Dawson, L. A. Kopff, L. Zhu, R. J. McMahon, L. Yu, R. Richert, and M. D. Ediger, J. Chem. Phys. 136, 094505 (2012).
- [34] S. S. Dalal, A. Sepúlveda, G. K. Pribil, Z. Fakhraai, and M. D. Ediger, J. Chem. Phys. 136, 204501 (2012).
- [35] H. Vogel, Phys. Z. 22, 645 (1921).
- [36] G. S. Fulcher, J. Am. Ceram. Soc. 8, 339 (1925).
- [37] G. Tammann and W. Hesse, Z. Anorg. Allg. Chem. **156**, 245 (1926).
- [38] J. H. Magill and A. R. Ubbelohde, Trans. Faraday Soc. 54, 1811 (1958).
- [39] D. J. Plazek and J. H. Magill, J. Chem. Phys. 45, 3038 (1966).
- [40] D. J. Plazek and J. H. Magill, J. Chem. Phys. 49, 3678 (1968).
- [41] Please note that in the here cited study (studies) of Magill and Plazek the sample has been mislabeled as α, α, α -TNB [31].
- [42] J. H. Magill, J. Chem. Phys. 47, 2802 (1967).
- [43] J. H. Magill and D. J. Plazek, Nature 209, 70 (1966).
- [44] J. H. Magill and D. J. Plazek, J. Chem. Phys. 46, 3757 (1967).
- [45] K. L. Ngai, J. H. Magill, and D. J. Plazek, J. Chem. Phys. 112, 1887 (2000).
- [46] M. D. Ediger, C. A. Angell, and S. R. Nagel, J. Phys. Chem. **100**, 13200 (1996).
- [47] M. D. Ediger, P. Harrowell, and L. Yu, J. Chem. Phys. 128, 034709 (2008).
- [48] R. Richert, K. Duvvuri, and L.-T. Duong, J. Chem. Phys. 118, 1828 (2003).
- [49] S. F. Swallen, P. A. Bonvallet, R. J. McMahon, and M. D. Ediger, Phys. Rev. Lett. **90**, 015901 (2003).
- [50] D. Ehlich and H. Sillescu, Macromolecules 23, 1600 (1990).
- [51] F. Fujara, B. Geil, H. Sillescu, and G. Fleischer, Z. Phys. B: Condens. Matter 88, 195 (1992).
- [52] H. Sillescu, J. Non-Cryst. Solids 243, 81 (1999).
- [53] M. D. Ediger, Annu. Rev. Phys. Chem. **51**, 99 (2000).
- [54] I. Tsukushi, O. Yamamuro, T. Ohta, T. Matsuo, H. Nakano, and Y. Shirota, J. Phys.: Condens. Matter **8**, 245 (1996).

TABLE I: Properties of the TNB isomers in the glassy, crystalline and supercooled liquid states. $T_{\rm g}$ is the glass transition temperature, $T_{\rm m}$ is the melting temperature, and $\Delta H_{\rm m}$ and $\Delta S_{\rm m}$ are the melting enthalpy and entropy, respectively. The parameter ξ is the slope as obtained from linear fits to $\log(\tau_{u,\rm kin}/s)$ vs. $\log(\tau_{\alpha}/s)$ as shown in Fig. 8, where the covered temperature range is indicated, too (values normalized by $T_{\rm g}$). The standard deviation of ξ and the correlation coefficient R^2 are provided as measures for the quality of the fit. The steepness index m is also tabulated.

System	Glass		Crystals					Supercooled Liquid		
	T _g ^a	T _m ^b	T _m c	T _m d	$\Delta H_{ m m}^{-d}$	$\Delta S_{ m m}/R^{ m e}$	Slope ξ of $\log(\tau_{u,kin}/s)$ vs. $\log(\tau_{\alpha}/s)^{f}$		m ^a	
	/ °C	/ °C	/ °C	/ °C	/ (kJ mol ⁻¹)		$T / T_{ m g}$	$\xi(\mathbb{R}^2)$		
α,α,α-ΤΝΒ	73.0	182	186	183	33.3	8.8	1.08-1.18	0.81±0.03 (0.995)	73.0	
α, α, β -TNB	71.4	194	197	199	41.9	10.7	1.10-1.23	0.743±0.005 (1.000)	85.9	
α,β,β -TNB	64.2	147	153	150	27.5	7.8	1.09-1.15	0.64±0.02 (0.998)	87.7	

^a From Vogel-Fulcher-Tammann fits to dielectric relaxation times reported in Ref. [33], using $T_g = T(\tau_\alpha = 100s)$ and $m = d[\log(\tau_\alpha/s)]/d[T_g/T]$ at $T = T_g$, respectively.

^b From DSC measurements (onset value) reported in Ref. [31].

^c From visual inspection using the optical microscope (this work).

^d As provided in Ref. [54] $(\alpha, \alpha, \alpha$ -TNB) and Ref. [44] $(\alpha, \alpha, \beta$ -TNB), respectively, and as obtained from DSC measurements $(\alpha, \beta, \beta$ -TNB, this work).

^e With $\Delta S_m = \Delta H_m / T_m$ (for ΔH_m and T_m see footnote d) and the the ideal gas constant R.

^f As following from the u_{kin} data plotted in Fig. 8.

$$\alpha, \alpha, \alpha$$
-TNB α, α, β -TNB α, β, β -TNB

FIG. 1: Lewis structures of the three *tris*-naphthylbenzene (TNB) isomers studied in this paper. In the case of α , α , β -TNB the α and β position on the naphthyl ring is marked. Naphthyl rings connected to the central benzene ring at the β position are emphasized in pink.

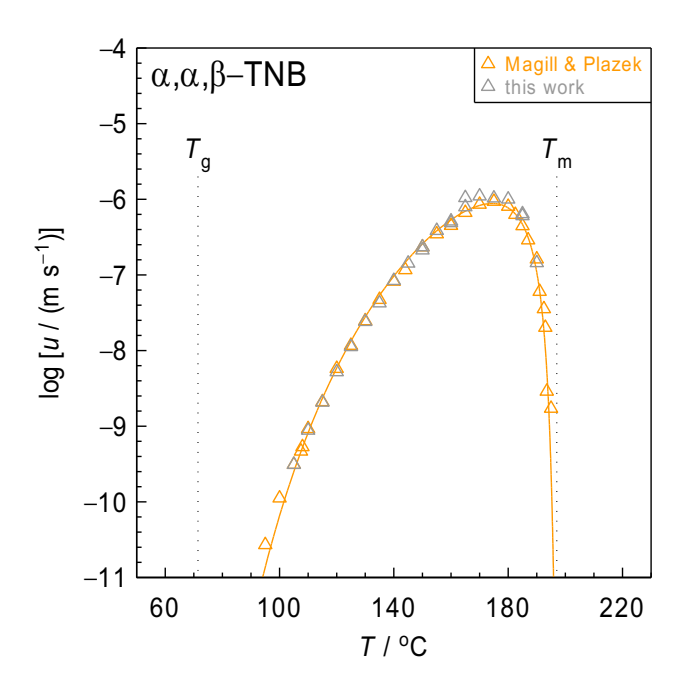


FIG. 2: Crystal growth rate u of α , α , β -TNB from this work and from a study by Magill and Plazek [41,44]. Orange triangles are the data from Table I in Ref. [44] and the orange solid line is defined by equation (7) provided in the same reference. Concerning the data of this work (gray triangles), each symbol represents the mean growth rate based on individual rates obtained for several growth sites. The size of the symbols is typically equal to or larger than twice the standard deviation. The dotted line marked $T_{\rm m}$ indicates the melting temperature as obtained in this work by visual inspection using the optical microscope. The dotted line marked $T_{\rm g}$ indicates the glass transition temperature as defined by $T_{\rm g} = T(\tau_{\alpha} = 100{\rm s})$, where the actual value of $T_{\rm g}$ has been calculated from the Vogel-Fulcher-Tammann equation for τ_{α} and the respective fit parameters provided in Table I in Ref. [33].

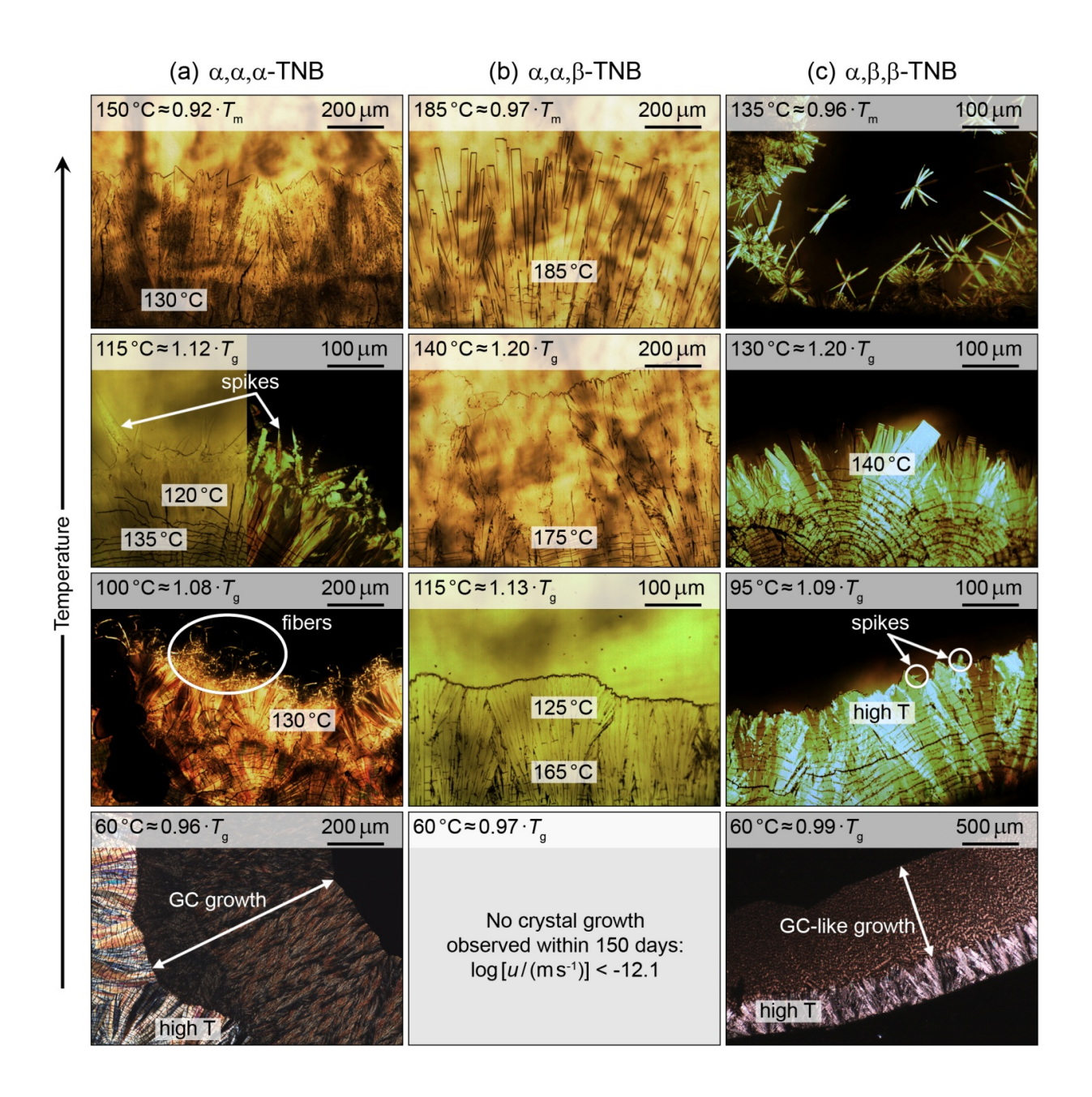
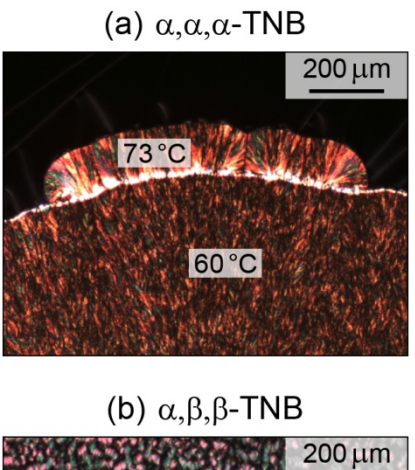


FIG. 3: Temperature-dependence of the growth morphology of the three TNB isomers. At the top of each photomicrograph the temperature at which it has been taken is stated. In the photograph itself information on crystalline regions grown at other temperatures is provided. In each case the upper edge of the letters approximately indicates the boarder to the subsequent region grown at another temperature. Furthermore, additional labels indicate the occurrence of fast growing spikes, fast growing loose fibers and GC or GC-like growth, respectively. Photographs with non-crystalline material (i. e., liquid or glassy TNB) appearing in black were recorded using crossed polarizers. Please note that tangentially (radially) oriented black lines in the crystalline regions are due to cracks (borders of single crystals). The crystalline material usually cracks when the sample is cooled to room temperature.



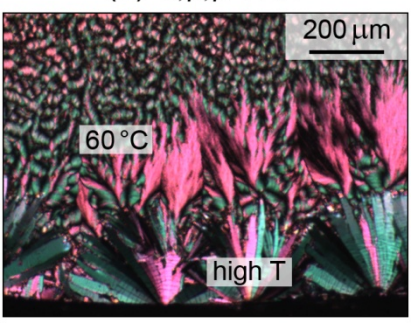


FIG. 4: (a) Crystals of α , α , α -TNB grown in the GC mode at 60 °C (\approx 0.96· T_g) and 73 °C (\approx 1.00· T_g), respectively. (b) Crystals of α , β , β -TNB grown in the normal mode at high temperature and in a GC-like mode at 60 °C (\approx 0.99· T_g).

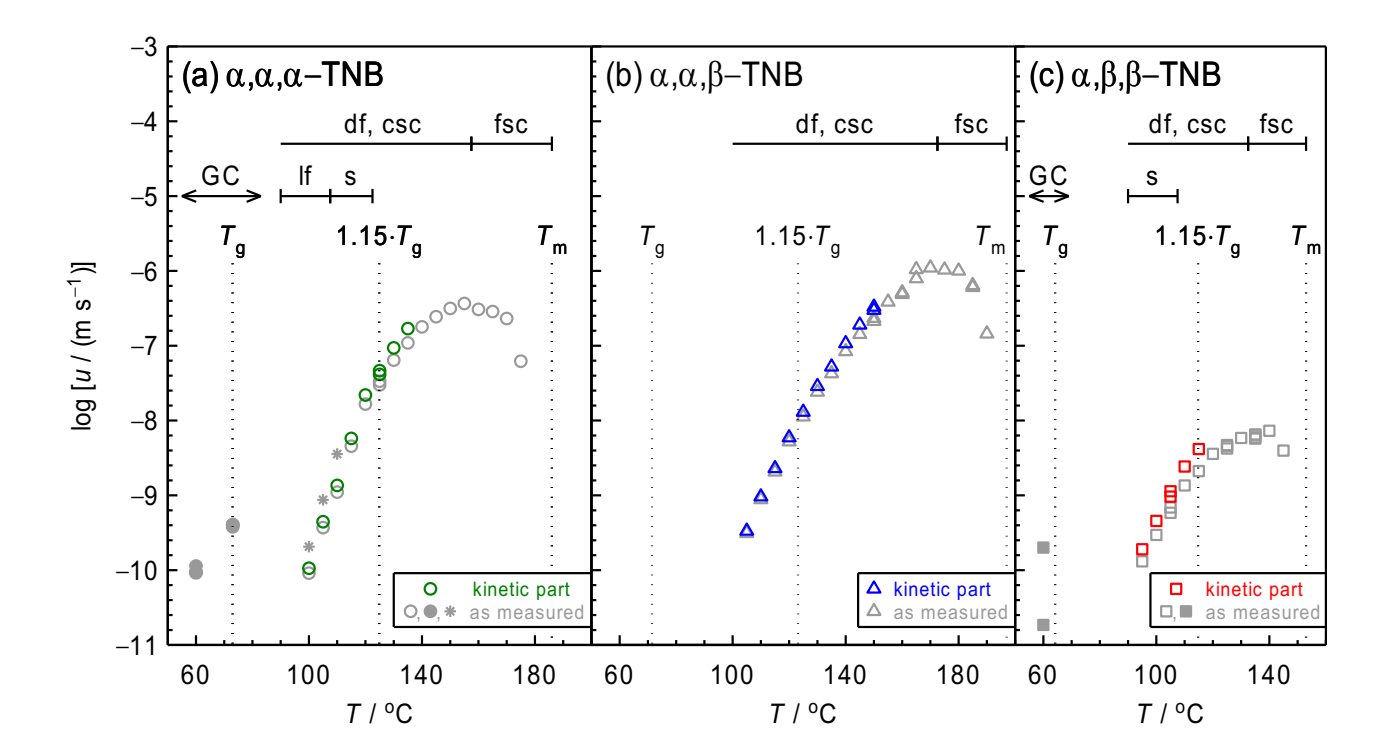


FIG. 5: Crystal growth rate u of the three TNB isomers. Empty symbols represent crystal growth in the normal mode, while full symbols indicate GC or GC-like growth. Asterisks refer to crystal growth which probably does not fill space (see main text). The kinetic part of u has been calculated using Eq. (3). Each symbol represents the mean growth rate based on individual rates obtained for several growth sites. The size of the symbols is typically equal to or larger than twice the standard deviation. In panel (c), two largely differing data points at 60 °C are shown. They refer to different temporal stages upon crystal growth which slows down with time (see main text). In each panel, the dotted line marked $T_{\rm m}$ indicates the melting temperature as obtained by visual inspection using the optical microscope. The dotted line marked T_g indicates the glass transition temperature T_g as defined by $T_g = T(\tau_\alpha = 100s)$, where the actual value of $T_{\rm g}$ has been calculated from the Vogel-Fulcher-Tammann equation for τ_{α} and the respective fit parameters provided in Table I in Ref. [33]. The dotted line marked $1.15 \cdot T_g$ indicates the typical temperature below which fast growing fibers were found to occur in systems showing GC growth (see main text). In the top part of each panel the preferred growth morphology is indicated. GC marks the glass-crystal growth mode or GC-like transient fast growth; If and s indicate the occurrence of fast growing loose fibers and spikes, respectively; df and csc mark compact growth of dense fibers and single crystals, respectively, and fsc marks the region where faceted single crystals grow.

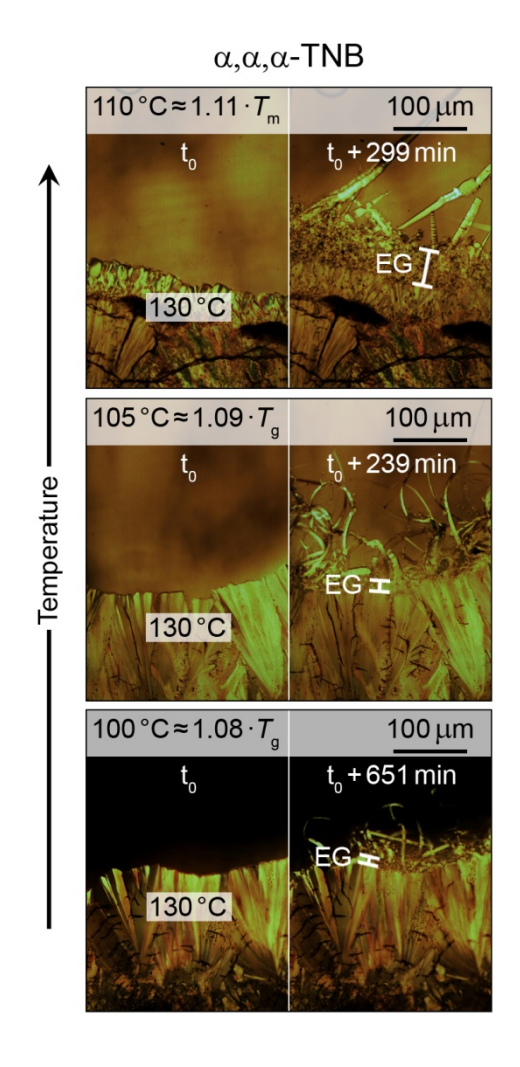


FIG. 6: Photomicrographs of α, α, α -TNB highlighting enhanced crystal growth (EG) at growth fronts from which fast growing spikes or fibers emanate. In each panel the left photograph was taken shortly after reaching the target temperature ($T_g < T < 1.15 \cdot T_g$, see the top of each panel), hence $t_0 \approx 0$, while the right photograph was taken at a later stage as indicated. In the left photographs information on crystal-line regions grown at another temperature is provided. In the right photograph we mark the distance by which the growth front has advanced into the liquid state in white. The corresponding crystal growth rates u are shown as asterisks in Fig. 5(a). Please note that the morphology of this somewhat enhance growth (as compared to the normal growth) has similarities with the morphology of the loose spikes or fibers.

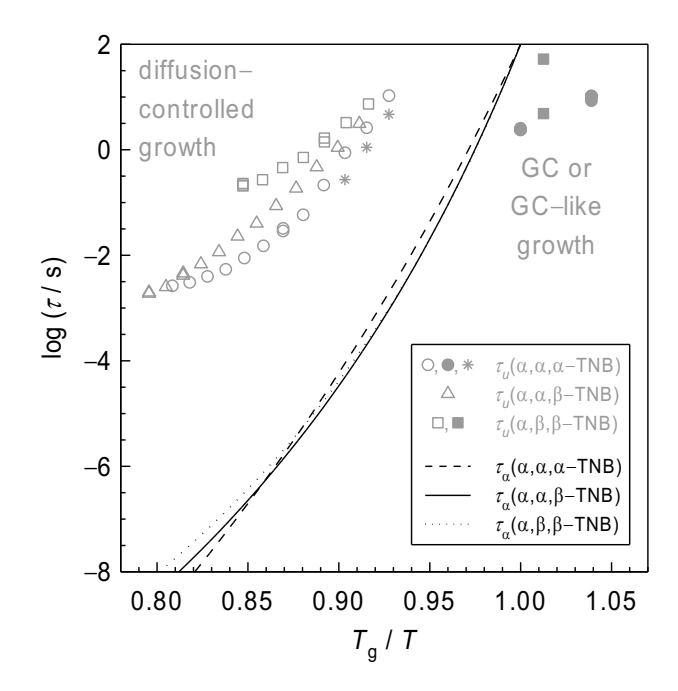


FIG. 7: Time scale of crystal growth (τ_u) and time scale of liquid relaxation (τ_α) of the three TNB isomers in an Arrhenius plot. The temperature is scaled by the glass transition temperature T_g as defined by $T_g = T(\tau_\alpha = 100\text{s})$, thus, $\log[\tau_\alpha(T_g)/\text{s}] = 2$. τ_α is obtained by dielectric relaxation spectroscopy, where the plotted function is given by a fit to the Vogel-Fulcher-Tammann equation [33]. τ_u is given by a/u with a being the molecular diameter [22] and u being the crystal growth rate as measured. Hence, τ_u is the time within which the crystal grows by one molecular layer. Empty symbols represent crystal growth in the normal mode, while full symbols indicate GC or GC-like growth. Asterisks refer to crystal growth which probably does not fill space (see main text). In the glass transition region $(T_g/T \approx 1)$ and at temperatures below T_g $(T_g/T > 1)$, GC (GC-like) growth is observed for α, α, α -TNB $(\alpha, \beta, \beta$ -TNB). For this crystal growth mode τ_u is smaller than τ_α and, contrary to the normal growth mode at higher temperatures, the crystallization kinetics is not controlled by diffusion.

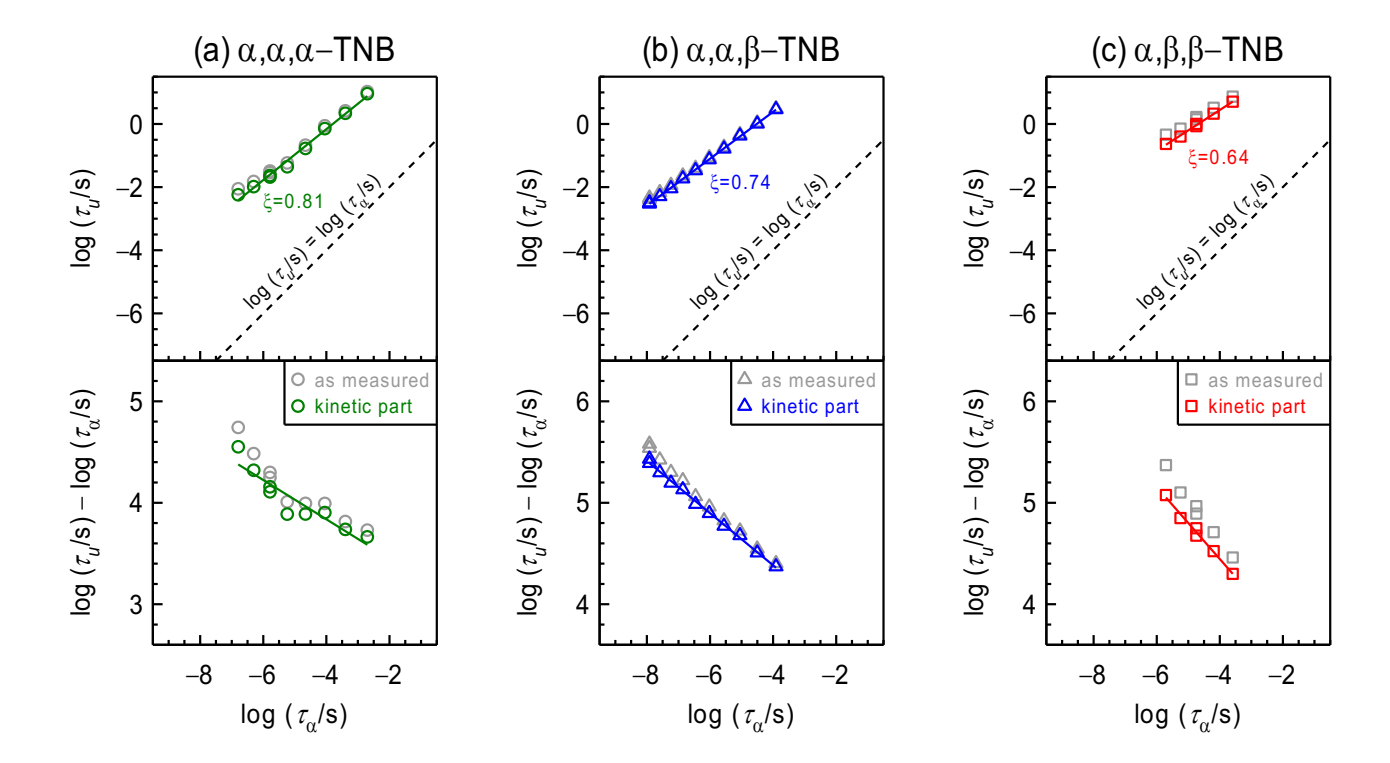


FIG. 8: Relation between the time scales of diffusion controlled crystal growth (τ_u) and liquid relaxation (τ_α) of the three TNB isomers. τ_u is given by a/u ($a/u_{\rm kin}$) with a being the molecular diameter [22] and u ($u_{\rm kin}$) being the crystal growth rate as measured (the kinetic part of the crystal growth rate). Hence, τ_u is the time within which the crystal grows by one molecular layer. τ_α is obtained by dielectric relaxation spectroscopy, where the actual numbers are calculated from the Vogel-Fulcher-Tammann equation and the fit parameters provided in Table I in Ref. [33]. The solid line in the top part of each panel is a linear fit to the data based on the kinetic part of the crystal growth rate; ξ is its slope. The dashed line is given by $\log(\tau_u/s) = \log(\tau_\alpha/s)$. This linear function has been subtracted from the data points and from the linear fit in the top part of each panel to gain the data plotted in the bottom part of each panel which emphasize the quality of the fit.